BIOCHEMISTRY
including biophysical chemistry & molecular biology
Article

*Biochemistry* **2009,** *48,* 12169–12179 12169
DOI: 10.1021/bi901686j

# The Structure of the UbcH8−Ubiquitin Complex Shows a Unique Ubiquitin Interaction Site[†]

Stephanie A. Serniwka and Gary S. Shaw*

*Department of Biochemistry, University of Western Ontario, London, Ontario N6A 5C1, Canada*

*Received June 10, 2009; Revised Manuscript Received November 19, 2009*

ABSTRACT: Ubiquitin-mediated proteolysis utilizes a series of three key enzymes (E1, E2, and E3) to transfer and then covalently modify a substrate with ubiquitin. E2 conjugating enzymes are central proteins in this pathway responsible for the acceptance of a ubiquitin from the E1 enzyme and association with an E3 protein. All E2 enzymes covalently bind ubiquitin through a thiolester linkage between a conserved active-site cysteine on E2 and the C-terminal glycine on ubiquitin. It is not known whether E2 enzymes utilize similar surfaces and residues to coordinate a ubiquitin molecule and how this might contribute to any substrate specificity. In this work, we determined the structure of the human E2 enzyme UbcH8 (UBE2L6) covalently bound to ubiquitin by NMR spectroscopy. A disulfide bond mimicking the short-lived thiolester was formed between the two proteins providing a stable complex. Overall, the structure of UbcH8 does not undergo a significant conformational change upon forming a complex with ubiquitin. Chemical shift perturbation and cross-saturation experiments were used to identify contacts between UbcH8 and ubiquitin and those contacts used as inputs for HADDOCK molecular docking to produce the structure of the UbcH8−ubiquitin complex. An ensemble of 16 structures (root-mean-square deviation of 0.83 Å) showed that ubiquitin interacts with the linker region prior to the α5 helix as well as residues near the catalytic site. This region corresponds to an area of negative potential on the UbcH8 surface and is considerably different from other E2−ubiquitin interaction sites. Our findings indicate the positioning of ubiquitin on UbcH8 would still allow interaction with E1 and E3 enzymes. Together, the results suggest the UbcH8−ubiquitin complex may provide an additional level of specificity in the ubiquitination pathway.

The mechanism of protein degradation by the ubiquitination pathway plays a vital intracellular role in preserving homeostasis. Ubiquitin-mediated proteolysis ensures that short-lived, damaged, or denatured proteins, involved in numerous cellular processes such as cell-cycle control, DNA repair, and signaling, are removed from the cell (*1*). Through a series of enzymatic reactions involving an E1 activating enzyme, an E2 conjugating enzyme, and an E3 ligase, multiple ubiquitin (Ub)[1] molecules are covalently attached to a target protein substrate destined for degradation by the 26S proteasome (*2*). Briefly, E1 first binds Ub in an ATP-dependent reaction. The Ub is then transferred to E2, forming a thiolester linkage between the catalytic cysteine on E2 and the C-terminal glycine (G76) on Ub. Depending on whether a RING or HECT E3 ligase is involved, the Ub is either directly passed from E2 to the ε-amino group of a lysine on the target substrate or first linked to HECT E3 and then transferred to the target substrate (*1*). Formation of a poly-Ub chain targets the substrate to the 26S proteasome for degradation. Due to the critical nature of ubiquitination in cellular regulation, mutations in the enzymatic machinery have been implicated in some neurodegenerative diseases, including Parkinson's (*3*). Enzyme specificity within ubiquitination plays a major role in substrate recognition and targeting. Overall in humans, there are one E1, more than 25 E2s, and hundreds of E3 ligases (*4*). Specificity arises since an E2 will interact and function with only certain E3s. For instance, the human E2 UbcH8 (UBE2L6) interacts with E3s Parkin and E6AP, while a related E2, UbcH5, has been shown to bind E3s BRCA1-BARD1 and Rsp5 (*5*−*7*). This particular E2−E3 interaction can then dictate which subset of targets are ubiquitinated in the pathway.

By forming a thiolester intermediate with Ub, followed by recognition and association with an E3, E2-conjugating enzymes are central components in the transfer of Ub to the target substrate. A structurally conserved catalytic domain containing the active-site cysteine involved in formation of a thiolester with G76 of Ub is found across all E2s. Recently, it was shown that although E2s are well conserved across families, there is a high level of active-site diversity in terms of both its structural features and sequence (*8*) and the surface charge balance (*9*, *10*). For example, the active-site cysteine present in all E2s occupies a variety of spatial positions within the catalytic fold of the enzyme. Furthermore, it was noted that sequence variations significantly affect the electrostatic properties of the catalytic region and the surrounding surfaces of different E2 enzymes. Finally, a conserved polar residue (often Asn or His) located upfield from the active-site cysteine has been suggested not only to stabilize the oxyanion hole during substrate lysine attack on the thiolester-bound Ub but also to strategically locate the C-terminal tail of Ub for substrate attachment (*8*). These combined results indicate that different E2 enzymes may uniquely position the thiolester-linked

[†]This work was supported by research grants from the Canadian Institutes of Health Research, the Canadian Cancer Society, and the Canada Research Chairs Program (G.S.S.) and by a Canadian Institutes of Health Research Doctoral Award (S.A.S.).

*To whom correspondence should be addressed. Phone: (519) 661-4021. Fax: (519) 661-3175. E-mail: gshaw1@uwo.ca.

[1]Abbreviations: Ub, ubiquitin; $Ub^{Cys}$, ubiquitin carrying a G76C substitution; UbcH8−$Ub^{Cys}$, UbcH8−$Ub^{Cys}$ disulfide complex; HADDOCK, high-ambiguity-driven biomolecular docking.


Published on Web 11/23/2009

Ub, providing an extra level of specificity for target protein recognition.

Despite the importance of the E2−Ub thiolester intermediate, there are currently only two structural models of the complex available. The first model of an E2−Ub intermediate, Ubc1−Ub, was created by forming the thiolester linkage directly in the NMR tube prior to peak intensity analysis and subsequent model building (*11*). In this structure, a truncated form of the class II E2 enzyme, Ubc1, was used in which the C-terminal Ub-associated domain was deleted (*11*). More recently, Eddins et al. (*37*) determined the crystal structure of the Mms2/Ubc13−Ub complex by substituting the active-site cysteine in Ubc13 with a serine (C87S) and forming a covalent ester bond with G76 of Ub. In this structure, the position of the Ub is dictated by interactions not only with Ubc13 but also with the ubiquitin enzyme variant protein Mms2. A comparison of these two structures shows that the Ub is oriented differently with respect to the E2 enzyme, perhaps reinforcing the idea that differential arrangements of the Ub on an E2 enzyme may play a role in specificity in the ubiquitination pathway.

UbcH8 (UBE2L6) is a human E2-conjugating enzyme (*12*) that possesses the classic $\alpha/\beta$ E2 fold for its catalytic domain. In vitro studies have shown that UbcH8 interacts with the RING E3 ligase parkin, a protein that has been implicated in the onset of autosomal recessive juvenile Parkinsonism (*13*). Unlike Ubc1 or Ubc13, UbcH8 is a canonical class I E2 enzyme containing only a catalytic domain and no C-terminal extension (Ubc1) or requirement for a ubiquitin enzyme variant (Ubc13/Mms2) to function. In this work, we have assembled the UbcH8−Ub intermediate using a stable disulfide linkage between the C-terminus of Ub and the active-site cysteine in UbcH8. NMR studies have shown the disulfide linkage is an excellent structural mimic for the thiolester. This approach allowed the first complete characterization of the UbcH8−Ub complex to be conducted by NMR spectroscopy. Chemical shift perturbation and cross-saturation experiments in conjunction with molecular docking were used to determine the structure of the UbcH8−Ub intermediate. This structure provides details that show how this class I E2 enzyme uniquely coordinates Ub.

## EXPERIMENTAL PROCEDURES

*Protein Expression and Purification*. The full-length UbcH8 DNA template was provided by P. Robinson (University of Leeds, Leeds, U.K.) in the pET3a expression vector. UbcH8 contains three cysteine residues: the catalytic thiolester-forming cysteine (C85) and two additional cysteines, Cys97 and Cys101. To prevent disulfide formation during structural studies, Cys97 and Cys101 were mutated to serines using QuikChange site-directed mutagenesis (Stratagene, La Jolla, CA). A K48R substituted version of Ub was used in all experiments. This protein also has the C-terminal glycine replaced with cysteine ($Ub^{Cys}$) for formation of the disulfide complex with UbcH8. Both His-tagged UbcH8 (C97,101S) and $Ub^{Cys}$ were expressed in *Escherichia coli* strain BL21(DE3). $^{15}N$- and $^{13}C$-labeled $Ub^{Cys}$ and unlabeled $Ub^{Cys}$ were expressed and purified as described previously (*14*). $^{15}N$- and $^{13}C$-labeled UbcH8 was overexpressed by induction with 0.4 mM IPTG in M9 medium containing $^{15}NH_4Cl$ and [$^{13}C$]glucose. $^{2}H$- and $^{15}N$-labeled UbcH8 and $Ub^{Cys}$ were grown in increasing concentrations of $D_2O$ (0, 75, and 100%) with [$^{2}H$,$^{12}C$]glucose and $^{15}NH_4Cl$ to allow bacteria to adapt to growth in deuterated media (*15*). Expression was induced at an $OD^{600}$ of 0.4 with 0.4 mM IPTG and continued for 18−20 h. [$^{2}H$,$^{15}N$]$Ub^{Cys}$ was purified as described previously (*14*). Cells containing either $^{2}H$- and $^{15}N$-labeled, $^{15}N$- and /$^{13}C$-labeled, or unlabeled UbcH8 were lysed with a French pressure cell and centrifuged to isolate the soluble component. UbcH8 was purified with the HisTrap-FF affinity column on an AKTA FPLC system and eluted with 500 mM imidazole (GE Healthcare). Cleavage of the His tag was achieved by dialyzing the eluted UbcH8 at 4 °C in buffer containing Tobacco Etch Viral enzyme. The purity and integrity of both $Ub^{Cys}$ and UbcH8 (C97,101S) were confirmed by SDS−PAGE and electrospray ionization mass spectrometry (for UbcH8, $MW_{obs}$ = 17799.35 Da and $MW_{calc}$ = 17799.58 Da; for Ub, $MW_{obs}$ = 8638.74 Da and $MW_{calc}$ = 8638.95 Da) (Biological Mass Spectrometry Laboratory, University of Western Ontario).

*Formation of the UbcH8−Ub Disulfide Complex*. Formation of a disulfide between ~0.1 mM labeled UbcH8 and unlabeled $Ub^{Cys}$ was conducted via dialysis treatments in buffer containing $CuCl_2$ as previously described (*14*). The UbcH8−$Ub^{Cys}$ complex was purified by passage through a Sephadex G75 size exclusion column (GE Healthcare). Fractions containing pure UbcH8−$Ub^{Cys}$ were confirmed by nonreducing SDS−PAGE and pooled for subsequent NMR experiments. The identity of UbcH8−$Ub^{Cys}$ was confirmed using electrospray ionization mass spectrometry (for [$^{2}H$/$^{15}N$]UbcH8−$Ub^{Cys}$, $MW_{obs}$ = 27631.9 Da and $MW_{calc}$ = 27631.3 Da)

*NMR Spectroscopy*. All NMR data were acquired at 25 °C on Varian INOVA 600 MHz (University of Western Ontario) or Varian INOVA 800 MHz spectrometers (NANUC, Edmonton, AB) equipped with triple-resonance cold probes and *z*-gradients. For the NMR resonance assignments of UbcH8, samples of 0.5 mM uniformly labeled [$^{15}N$/$^{13}C$]UbcH8 were prepared in 20 mM $NaHPO_4$ (pH 7), 1 mM EDTA, 1 mM DTT, 50 mM Arg, 50 mM Glu, and 100 mM NaCl (10% $D_2O$/90% $H_2O$). The Arg/Glu buffer was used to prevent aggregation during concentration steps (*16*). The following experiments were conducted for sequential backbone assignment of UbcH8: $^{1}H-^{15}N$ HSQC, $^{1}H-^{13}C$ HSQC (*17*), CBCA(CO)NH, HNCO (*18*), HNCACB (*19*), C(CO)NH, and H(CCO)NH (*20*). All data were processed using NMRPipe and NMRDraw (*21*) and analyzed with NMRView (*22*).

NMR samples of both [$^{15}N$/$^{13}C$]UbcH8−$Ub^{Cys}$ and UbcH8−[$^{15}N$/$^{13}C$]$Ub^{Cys}$ complexes were prepared in the same buffer described above, excluding DTT. $^{1}H-^{15}N$ HSQC, CBCA(CO)NH, and HNCACB spectra were collected to assign the backbone atoms of the disulfide complexes. Amide chemical shift deviations were calculated for each residue and normalized according to the relationship $\sum\Delta\delta = |\Delta\delta(^{1}H)| + |(0.2)\Delta\delta(^{15}N)|$, where $\Delta\delta(^{1}H)$ and $\Delta\delta(^{15}N)$ are the chemical shift differences between the free and disulfide-bound states (*23*).

Cross-saturation NMR experiments were conducted at 600 or 800 MHz as described by Takahashi et al. (*33*) on 0.35 mM [$^{2}H$/$^{15}N$]UbcH8−$Ub^{Cys}$ and [$^{2}H$/$^{15}N$]$Ub^{Cys}$−UbcH8 complexes in 20 mM $NaHPO_4$ (pH 7) buffer, as described above. Control $^{1}H-^{15}N$ HSQC spectra were recorded with an off-resonance pulse centered at −12.0 ppm. Saturation of aliphatic protons on the unlabeled component of the disulfide complex was performed using the WURST-2 decoupling scheme at a saturation frequency of 0.9 ppm (*24*). A range of experiments was conducted at 600 MHz using saturation pulses of 200, 400, 800, and 1600 ms and an appropriate relaxation delay to give a total time of 3200 ms (saturation pulse plus delay) for both complexes. A single saturation transfer experiment was conducted at 800 MHz

for [$^2$H/$^{15}$N]UbcH8−Ub$^{Cys}$ using an 1800 ms saturation pulse and corresponding relaxation delay.

*HADDOCK Docking Protocol*. The docking program HADDOCK version 2.0 (*34*) was used to calculate the structure of the UbcH8−Ub$^{Cys}$ complex. Chemical shift perturbation results, cross-saturation data, and the disulfide linkage were used as restraints in the docking process. Structures for docking were taken from the Protein Data Bank (PDB): entry 1WVZ for UbcH8 and entry 1UBQ for Ub (*25*). Solvent accessibilities of all residues from UbcH8 and Ub$^{Cys}$ were calculated with NACCESS (*26*). Active residues were selected as those residues that experienced a chemical shift change in the complex, relative to the free proteins, that was greater than one standard deviation above the average change ($>0.083$ ppm for UbcH8 and $>0.059$ ppm for ubiquitin) or a reduction in amide peak intensity of $>10\%$ that could be fit with an exponential decay from the cross-saturation experiments and displayed $>50\%$ surface accessibility. Passive residues were neighboring residues of active residues that also exhibited high surface accessibility. The experimentally derived data were classified as ambiguous interaction restraints (AIR) with a maximum effective distance of 5.0 Å. Restraints were included for active−active and active−passive residue groups but not passive−passive groups. The disulfide linkage between the thiol groups for C85 (UbcH8) and C76 (Ub$^{Cys}$) was defined as an unambiguous interaction restraint with a distance restraint range of 2.0−3.0 Å. The force constant for the AIR restraints was set to 10 kcal mol$^{-1}$ Å$^{-2}$, while the force constant for the unambiguous interaction restraint was increased to 50 kcal mol$^{-1}$ Å$^{-2}$ for all stages of docking. Initially, rigid body minimization calculated 1000 structures. From this calculation, 200 of the lowest-energy structures were then subjected to semiflexible simulated annealing and refinement in explicit solvent. The final structure solutions were clustered using a pairwise backbone root-mean-square deviation (rmsd) cutoff of 2.0 Å. The disulfide bond was introduced into the docked proteins by manually rotating the cysteine C$\alpha$−C$\beta$ bonds to place the thiols within bonding distance. WHATIF (*27*) and PISA [Protein interfaces, surfaces and assemblies service (http://www.ebi.ac.uk/msd-srv/prot_int/pistart.html) (*28*)] were used to analyze the UbcH8−Ub$^{Cys}$ structures and binding interfaces. The mean representative structure was generated by MOLMOL (*29*). All structure figures were produced with PyMOL (*30*).

*Data Deposition*. Chemical shift assignments for the E2-conjugating enzyme UbcH8 are deposited in the BioMagResBank as accession number 16321. Coordinates of the 16 best UbcH8−Ub$^{Cys}$ models, selected from HADDOCK, have been deposited in the Protein Data Bank (entry 2KJH).

## RESULTS

In the ubiquitination pathway involving the E2-conjugating enzyme UbcH8 (UBE2L6), a thiolester is formed between UbcH8 and Ub. In previous studies using Ubc1, we have shown that this thiolester complex can be unstable, especially for longer-term structural studies. To increase the stability of the UbcH8−Ub$^{Cys}$ covalent complex, we opted to form a disulfide linkage between the catalytic cysteine of UbcH8 (C85) and a cysteine-substituted derivative of Ub in which G76 was replaced with cysteine (Ub$^{Cys}$). Formation of the E2−Ub disulfide has been previously demonstrated for Ubc1, UbcH7 (UBE2L3), and Ubc13 (UBE2N). Further, NMR experiments have shown that the $^1$H−$^{15}$N HSQC spectrum of the Ubc1−Ub disulfide is nearly identical to that of the thiolester but the disulfide has the added advantage of fewer side products during preparation and greater long-term stability (*14*).

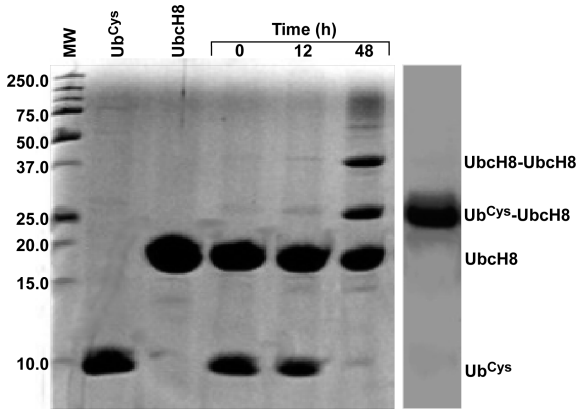


FIGURE 1: Nonreducing SDS−PAGE of formation of the ubiquitin−UbcH8 disulfide. UbcH8 and ubiquitin (Ub$^{Cys}$) were reduced in the presence of TCEP prior to dialysis treatment with $CuCl_2$. Disulfide formation (UbcH8−Ub$^{Cys}$) was monitored by nonreducing SDS−PAGE over 48 h until Ub$^{Cys}$ in the reaction mixture was exhausted. The UbcH8−Ub$^{Cys}$ complex was purified by size exclusion chromatography, as shown in the gel inset. The identity of the complex was confirmed by electrospray ionization mass spectrometry (for [$^2$H/$^{15}$N]UbcH8−Ub$^{Cys}$, $MW_{obs}$ = 27631.9 Da and $MW_{calc}$ = 27631.3 Da).

*Formation of the UbcH8−Ub$^{Cys}$ Disulfide Intermediate*. Prior to disulfide formation, two additional cysteines in UbcH8 (C97 and C101) were substituted with serine residues to direct the disulfide formation with Ub$^{Cys}$ solely toward the active-site cysteine (C85) residue in UbcH8. The stable disulfide complex mimicking the E2−Ub thiolester intermediate was formed between UbcH8 and Ub$^{Cys}$ using dialysis treatment versus a $CuCl_2$ buffer over 48 h (Figure 1). The byproducts of the oxidation reaction were removed using size exclusion chromatography yielding purified UbcH8−Ub$^{Cys}$. This complex remained stable for more than 60 days after the reaction (Figure 1).

The interaction between UbcH8 and Ub proteins in the UbcH8−Ub$^{Cys}$ complex was assessed by NMR spectroscopy to determine whether any major structural changes occurred in the UbcH8 or Ub$^{Cys}$ proteins upon formation of the complex. This required the complete resonance assignment of UbcH8 and UbcH8−Ub$^{Cys}$ using standard triple-resonance experiments. The $^1H^N$ and $^{15}$N backbone amide resonances for 130 of 134, and 128 of 134, non-proline residues were assigned for UbcH8 in the free and UbcH8−Ub$^{Cys}$ proteins, respectively (Figure 2A,B), along with 96% of the C$\alpha$, C$\beta$, and CO resonances. Chemical shift index analysis for UbcH8 shows excellent agreement between the secondary structure of UbcH8 in solution compared to that in the crystal structure [PDB entry 1WZV (Figure 2C)]. Upon formation of the UbcH8−Ub$^{Cys}$ complex, peak broadening was observed for many resonances indicative of a larger species present in the sample (Figure 2B). However, the chemical shift index for the E2 protein in UbcH8−Ub$^{Cys}$ showed a pattern of secondary structure similar to that of both UbcH8 in solution and UbcH8 in the crystal structure (Figure 2C). Similar results were obtained from the analysis of Ub$^{Cys}$ in the absence of and in complex with UbcH8 (not shown). These results show that no major changes in secondary structure occurred in either E2 or Ub$^{Cys}$ upon formation of the disulfide complex. A similar observation has been made for both Ubc1 and Ubc13 upon complexation with ubiquitin (*14*, *37*).

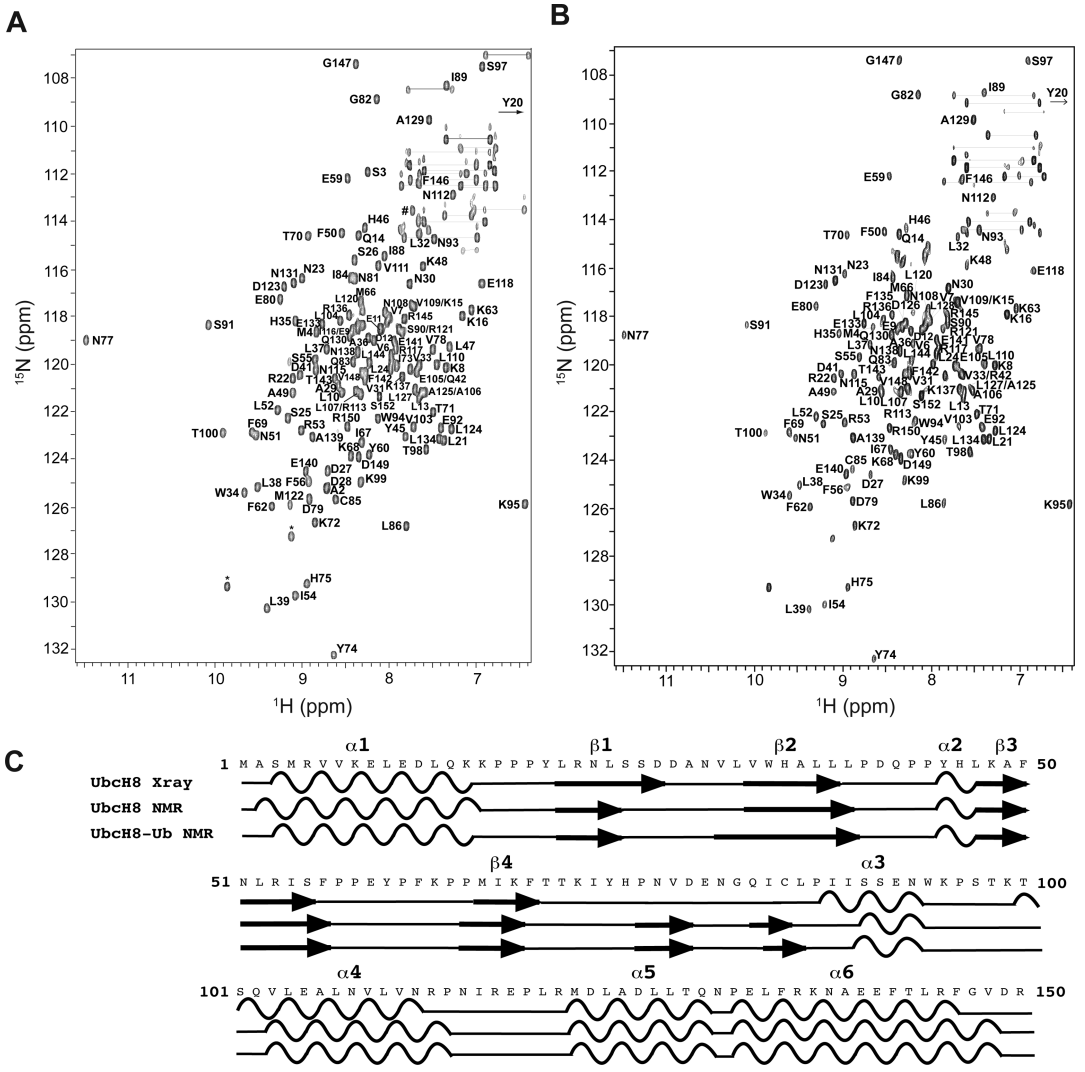


FIGURE 2: UbcH8 and UbcH8−Ub$^{Cys}$ have similar secondary structures. (A) $^{1}$H−$^{15}$N HSQC spectra of 0.5 mM uniformly $^{15}$N-labeled UbcH8 and (B) 0.35 mM UbcH8−Ub$^{Cys}$ prepared using uniformly $^{15}$N-labeled UbcH8. In both spectra, assignments were completed using standard triple-resonance techniques and labeled according to the one-letter amino acid code and residue number for UbcH8. Both samples were prepared in 20 mM $NaHPO_4$, 1 mM EDTA, 50 mM arginine, 50 mM glutamic acid, and 100 mM NaCl (pH 7). Spectra were recorded at 25 °C using a Varian Inova 600 MHz NMR spectrometer. Peaks connected with lines indicate side chain amide resonances. Peaks marked with an asterisk are tryptophan side chain amides; the peak marked with a number sign could not be assigned. (C) Secondary structure comparison of UbcH8 and UbcH8−Ub$^{Cys}$. The secondary structure of UbcH8 was derived from the X-ray coordinates (PDB entry 1WZV) and indicated as α-helix (waves) or $\beta$-sheet (arrows) structural elements above the protein sequence. The secondary structures for UbcH8 and UbcH8−Ub$^{Cys}$ in solution were identified using the chemical shift index (*43*) from assigned Hα, Cα, and CO chemical shifts of UbcH8.

*Mapping the Interaction of UbcH8−Ub$^{Cys}$ by Chemical Shift Perturbation Analysis*. The assigned spectra for UbcH8, Ub$^{Cys}$, and UbcH8−Ub$^{Cys}$ allowed chemical shift perturbations in UbcH8 and Ub$^{Cys}$ to be used to identify residues involved at the UbcH8−Ub$^{Cys}$ interface upon complex formation (Figure 3A; data not shown for Ub$^{Cys}$). As expected, the most striking chemical shift perturbations occurred for C85 in UbcH8 and C76 in Ub$^{Cys}$, which experienced amide nitrogen chemical shift changes of 1.280 and 0.243 ppm, respectively (Figure 3A). These large changes reflect the formation of the covalent bond between the two residues and the modifications of their local chemical environments from the reduced to the oxidized states. Two residues were observed to broaden significantly upon formation of a complex in UbcH8 (L47 and M122), probably indicating that these residues are directly at the protein−protein interface (M122) or are indirectly affected by residues that underwent significant chemical shift changes (L47). Several other residues in UbcH8 experienced chemical shift changes greater than one standard deviation above the average (Figure 3B). These residues were filtered for those showing > 50% surface accessibility to identify surface residues important for the ubiquitin interaction. This analysis showed that E80 and N81 (turn region prior to the catalytic cysteine), S90 (α3), and I116, E118, and L120 (α4−α5 loop) (Figure 3B) were most responsive to the formation of the UbcH8−Ub complex. These residues mapped to the region surrounding the catalytic C85 residue on UbcH8 similar to those observed in NMR studies of UbcH5c (*31*) and Ubc2b (*32*). It was noted that prior to screening of residues for surface accessibility, chemical shift changes were evident in the $\beta$1, $\beta$2, and $\beta$3 regions (e.g., S25, N30, V33, and H35) on the opposing side of E2 (Figure 3B), similar to those observed to undergo chemical shift changes upon noncovalent interaction of UbcH5c with Ub (*31*). However, unlike UbcH5c, UbcH8 is not capable of a noncovalent interaction with Ub$^{Cys}$ at concentrations up to 0.5 mM (data not shown). Other residues such as L52 and I54 were also filtered out since they are completely buried. These results indicate that

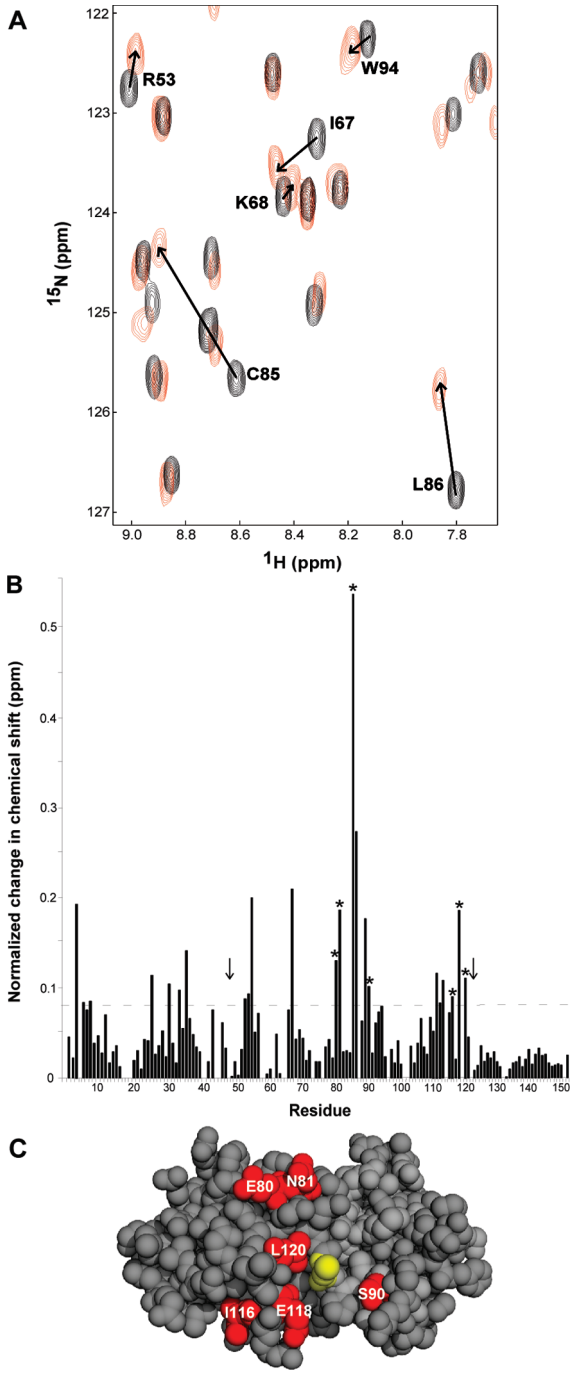


FIGURE 3: Interaction surface on UbcH8 in UbcH8−Ub$^{Cys}$ identified from chemical shift perturbation. (A) Expanded regions of the 600 MHz $^{1}$H−$^{15}$N HSQC spectra for 0.35 mM uniformly $^{15}$N-labeled UbcH8 alone (black contours) and in the UbcH8−Ub$^{Cys}$ complex (red contours). Peaks displaying chemical shift changes are labeled by residue and identified with arrows. (B) Bar graph of normalized amide chemical shift changes per residue for UbcH8 alone and in the UbcH8−Ub$^{Cys}$ complex. Amide chemical shift changes were normalized using the equation $\sum\Delta\delta = |\Delta\delta(^{1}H)| + |(0.2)\Delta\delta(^{15}N)|$. Residues that could not be assigned in UbcH8 (I73, S101, and Q102) are not shown and in the UbcH8−Ub$^{Cys}$ complex (L47 and M122) are indicated (arrows). The dotted line indicates the threshold for significant chemical shift changes (0.083 ppm, average + one standard deviation). Residues that had significant chemical shift changes and displayed >50% surface accessibility are identified with asterisks. (C) Surface representation of UbcH8 with residues from panel B that showed significant chemical shift changes upon formation of UbcH8−Ub$^{Cys}$ and possessed >50% surface accessibility colored red. The catalytic cysteine (C85) is colored yellow.

the chemical shift changes observed for some nonsurface residues likely result from secondary effects upon complexation with Ub$^{Cys}$, a conclusion similar to that suggested for UbcH5c (*31*). Residues that underwent significant chemical shift changes for Ub$^{Cys}$ and showed >50% surface accessibility were located in $\beta$2 (T14), the $\alpha$1 subsequent loop (D32, K33, and E34), and the C-terminal tail (C76).

*UbcH8−Ub$^{Cys}$ Binding Interface Assessed by Cross-Saturation Experiments*. The use of chemical shift perturbations to identify binding sites on proteins is a well-known and popular method. However, amide chemical shifts are sensitive to other secondary effects such as minor changes in buffer and pH conditions or hydrogen bonding patterns (*33*). These can lead to incomplete or inexplicable binding regions obtained on proteins. An alternate NMR technique for mapping binding interfaces between proteins is the cross-saturation experiment (*33*), involving the use of a proton-selective saturation pulse on an unlabeled component of the complex. The subsequent cross relaxation to the amide protons on an otherwise deuterated partner is monitored by decreases in peak intensities in the $^{1}$H−$^{15}$N HSQC spectra (*33*). Typical cross-saturation experiments by Takahashi and co-workers (*33*) have been conducted using >1 mM protein in 90% $D_2O$ to minimize spin diffusion among amide protons in the observation protein. In our case, the low concentration of the disulfide complex (350 $\mu$M) necessitated the use of 90% $H_2O$ to yield spectra with an adequate signal-to-noise ratio, although a more rigorous data analysis was needed to minimize artifacts resulting from spin diffusion artifacts.

Cross-saturation spectra for both [$^{2}$H,$^{15}$N]UbcH8 with unlabeled Ub$^{Cys}$ and unlabeled UbcH8 with [$^{2}$H,$^{15}$N]Ub$^{Cys}$ were recorded by comparing $^{1}$H−$^{15}$N HSQC spectra with saturation pulses at −12 ppm (control) and in the aliphatic proton region (0.9 ppm) (Figure 4). At long saturation pulse times (1800 ms), many residues exhibited decreases in intensity (Figure 4). Several of these residues exhibited a decreased intensity that was greater than average (K63, C85, S97, I88, I89, N115, R117, E118, and L120), suggesting these residues might be located near the E2−-Ub interface. However, it was also observed that many more peaks than expected exhibited some decreased peak intensity, making it difficult to determine which residues were near the protein interface and which ones were affected by spin diffusion. To identify residues at the UbcH8−Ub$^{Cys}$ interface and minimize the effects of spin diffusion, we collected $^{1}$H−$^{15}$N HSQC spectra over a range of saturation pulses up to 1600 ms and plotted the resulting peak intensities as a function of saturation pulse time (Figure 5A). When this approach was used, several residues exhibited peak intensity reductions up to 30% while others had little intensity change (Figure 5). To determine the residues affected most by cross saturation, peaks that decreased in magnitude >10% were fit with an exponential decay curve (Figure 5A). This approach clearly showed that some residues (C85, I116, and L120) had exponential decay rates from cross saturation that were obviously greater than those of others (K137), most likely indicating the decaying peaks represented residues near the protein−protein interface. Further, some residues exhibited plots with near-constant peak intensity at early saturation pulse times but decreased peak intensity during longer saturation times, likely a result of spin diffusion. This may account for the large number of residues that had apparent decreased peak intensities when only the longest saturation pulse time (1800 ms) was considered (Figure 4).

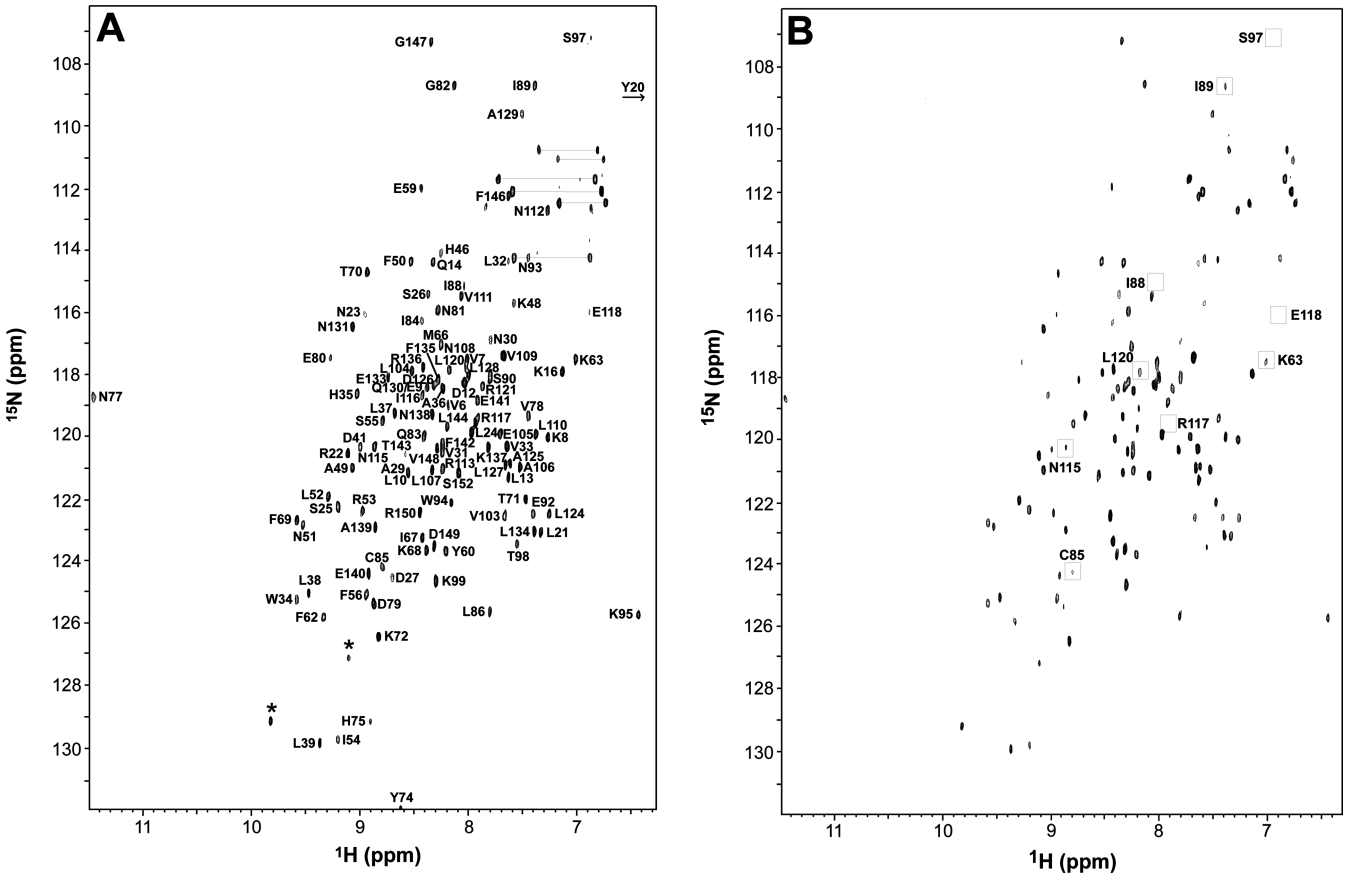


FIGURE 4: Cross-saturation spectra of the UbcH8−Ub$^{Cys}$ disulfide. $^{1}$H−$^{15}$N HSQC spectra of $^{2}$H- and $^{15}$N-labeled UbcH8 within the UbcH8−Ub$^{Cys}$ complex without (A) and with (B) irradiation of aliphatic protons at 0.9 ppm for 1800 ms. Sample resonances that exhibited the largest reductions in peak intensity are boxed in panel B. Spectra were recorded at 800 MHz using sample conditions described in the legend of Figure 2.

Residues at the UbcH8−Ub$^{Cys}$ interface were identified by plotting the rates for peak intensity reduction as a function of residue number (Figure 5B). As with the chemical shift perturbation data, these data were screened to select residues that had >50% surface accessibility (Figure 5B). These were mapped onto the surface of both UbcH8 (Figure 5C) and Ub using a similar approach (Figure S1 of the Supporting Information). For UbcH8, this showed several residues that were localized near the catalytic cysteine (C85), including residues in the linker preceding α2 (D41), α3 (S90 and E92), the loop connecting α3 and α4 (K95 and S97), and the loop connecting α4 and α5 (I116, R117, E118, and L120). A few more remote residues in $\beta$2 (F62 and K63) and the turn prior to the catalytic cysteine (T70 and K72) were also identified. Both the cross-saturation experiments and chemical shift mapping results (compare Figure 5C with Figure 3C) identified the α5 region comprising I116, E118, and L120 as a site of interaction. For Ub, the affected residues were T14 located in $\beta$2, Q31−G35 in the loop following α1, and C76 in the C-terminal tail. Cross-saturation and chemical shift perturbation results also compared well for Ub$^{Cys}$ with affected residues mapping to the C-terminal tail and $\beta$-sheet region. However, a more continuous binding surface was obtained on Ub$^{Cys}$ with the cross-saturation data (Figure S1 of the Supporting Information) as compared with the chemical shift data.

*Structure of the UbcH8−Ub$^{Cys}$ Complex*. Results from chemical shift mapping and cross-saturation NMR experiments and the crystal structures of UbcH8 and Ub (*25*) were used as input for the docking program HADDOCK to obtain a structural model of the UbcH8−Ub$^{Cys}$ complex (*34*). Ambiguous interaction restraints (AIR) identified from chemical shift mapping and cross-saturation transfer experiments were used to drive the docking process. For UbcH8, the selected residues (active residues) represented a composite of those in Figures 3C and 5C all having >50% surface accessibility. An identical approach was used for ubiquitin. Passive residues were also selected in this process as neighbors to active residues that also exhibited >50% surface accessibility. For UbcH8, this included four proline residues (P87, P96, P114, and P119) for which chemical shift and saturation transfer data were not available. It also included M122 positioned near the I116−E118−L120 cluster identified in both experiments and which underwent extreme line broadening upon complexation with ubiquitin. Overall, 16 active and 8 passive residues were selected for UbcH8 and 6 active and 8 passive residues for Ub$^{Cys}$ (Table 1). The numbers of active and passive residues for the docking process were similar to those in previous reports (*35*, *36*). In the UbcH8−Ub$^{Cys}$ complex, the disulfide between the active residues C85 on UbcH8 and C76 on Ub$^{Cys}$ was used as the single unambiguous interaction restraint in the docking procedure. This restraint greatly limited the range of locations sampled by the Ub$^{Cys}$ in the complex. Initially, 1000 structures were calculated, and 200 of the lowest-energy solutions were refined in explicit water. These 200 structures were clustered on the basis of a 2.0 Å rmsd, and the average intermolecular energies were used to rank the clusters, resulting in six clusters. The most populated cluster contained 56% of the structures (112 of 200), had on average 1.5 AIR violations of

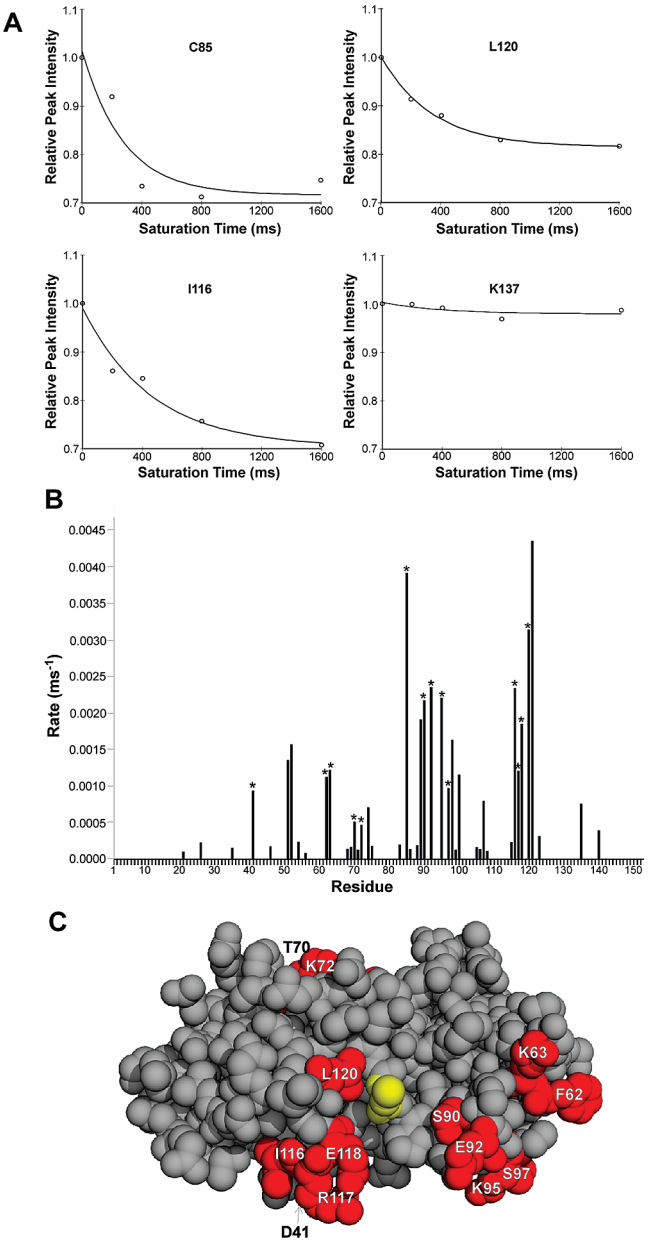


FIGURE 5: Interaction surface on UbcH8 in UbcH8−Ub$^{Cys}$ identified via saturation transfer experiments and rate analysis. (A) Decreases in relative peak intensities as a function of saturation pulse time (milliseconds) up to 1600 ms for representative UbcH8 residues. Data were collected at 600 MHz using sample conditions described in the legend of Figure 2. Data points were fit with a single-exponential decay curve. (B) Rates of the reduction in peak intensity per residue in UbcH8 as obtained from the exponential decay curve fits in panel A. Only residues that showed a >10% decrease in peak intensity were fit with a single-exponential curve and are shown in the plot. Residues that had the largest rates of decay and displayed >50% surface accessibility are marked with asterisks. (C) Surface representation of UbcH8 showing residues (red) marked with an asterisk in panel B that were identified as active residues and used for HADDOCK calculations. The catalytic cysteine (C85) is colored yellow.

>0.5 Å, and was also the cluster with the lowest average energy [−140 kcal mol$^{-1}$ (Table 2)]. Two other clusters contained 10.5 and 11% of the structures (21 and 22 of 200 each, respectively), with the three remaining clusters having 9 or fewer structures. The energies for the remaining clusters were broadly varied, with average energies ranging from −65 to −44 kcal mol$^{-1}$, nearly 100 kcal mol$^{-1}$ poorer than those for cluster 1 (Table 2). Further, alternative structures in the remaining clusters were marked by numerous AIR violations, demonstrating that the experimentally derived docking restraints were not satisfied. More importantly, four of the five remaining clusters did not satisfy the unambiguous disulfide restraint between C85 (UbcH8) and C76 (Ub), resulting in structures with S−S distances approaching 40 Å. Numerous runs of this docking procedure yielded similar results, with more than 50% of the final 200 calculated structure solutions falling into the same lowest-average energy cluster.

An ensemble of the 16 lowest-energy structures from the most populated cluster was selected as the best solution. The structures within this group satisfied all but one (either F62 or K63) active restraint and had favorable energies (Table 2). The structures displayed a high degree of similarity, having a backbone rmsd of 0.83 ± 0.26 Å with respect to the mean structure (Figure 6) for all secondary structure components in UbcH8 and Ub$^{Cys}$. In addition, all structures showed a S−S distance of 2.33 ± 0.19 Å between C85 in UbcH8 and C76 in Ub$^{Cys}$ indicative of a disulfide bond between the two proteins. The combined buried surface area of the UbcH8−Ub$^{Cys}$ interface was 815 ± 42 Å$^2$. The residues in UbcH8 with the largest decrease in surface accessibility (percentage) upon complexation with Ub$^{Cys}$ were C85, S90, and E92 in the turn preceding and within α3 and E118, P119, L120, and M122 located in the linker preceding the α5 region. Of these, S90, E118, and L120 exhibited both significant chemical shift changes and peak intensity reductions from the cross-saturation experiments. Residues in Ub$^{Cys}$ that experienced the highest percentage reduction in surface accessibility are T9, K11, and T14 in the linker following $\beta$1; E34, G35, and I36 in α1; and L71, R72, L73, R74, G75, and C76 located in the C-terminal tail. Together, these residues make up 78 and 60% of the binding surface on UbcH8 and Ub$^{Cys}$, respectively. The interface exhibits hydrophobic interactions between L71 and L73 on Ub$^{Cys}$ and L120 and M122 on UbcH8 as well as electrostatic contacts between K11 and R74 on Ub$^{Cys}$ and D126 and E92 on UbcH8, respectively. It was interesting to note that two key residues that form part of the UbcH8 binding interface with Ub precluded assignment by NMR experiments and related analyses (P119 and M122). In our analysis, these residues experienced the largest decreases in surface accessibility when in complex with Ub, indicating that M122 and P119 would be an integral part of the UbcH8−Ub binding surface.

On the basis of our cross-saturation NMR data, we noted residues that experienced decreases in intensity in the surrounding regions of the active-site cysteine. The HADDOCK models place Ub$^{Cys}$ near the linker region preceding α5 on UbcH8. Cross-saturation experiments noted a few residues on the opposing side of the active-site cysteine (F62, K63, K95, and S97) in the $\beta$3−$\beta$4 linker and α3−α4 linker (Figure 5C) that were not observed to shift in chemical shift perturbation data. These results could indicate that Ub$^{Cys}$ may be occupying an alternate position on UbcH8. One of the structural clusters calculated by HADDOCK does place Ub$^{Cys}$ in this vicinity. However, this cluster was poorly populated, with only 10.5% of the structures falling into this category. Moreover, the intermolecular energies for this cluster were unfavorable, and the solutions contained many AIR violations (six on average). Furthermore, of the 21 structures contained in this cluster, seven violated the required unambiguous S−S distance restraint (UbcH8$^{C85}$−Ub$^{C76}$). A more detailed inspection of the interface between UbcH8 and Ub$^{Cys}$ revealed that the Ub$^{Cys}$ C-terminal tail makes some important contacts with residues in α3 (Figure 6C) opposite the

Table 1: Intermolecular Restraints Used for the HADDOCK Docking Protocol

| | |
|---|---|
| ambiguous interaction restraints | |
| UbcH8 | |
| active residues[a] | D41, F62, K63, T70, K72, E80, N81, S90, E92, K95, S97, I116, R117, E118, L120 |
| passive residues[b] | E59, Q83, I84, P87, P96, P114, P119, M122 |
| ubiquitin | |
| active residues | T14, Q31, D32, K33, E34, G35 |
| passive residues | K11, T12, E16, A28, L71, L73, R74, G75 |
| flexible segment[c] | residues 71−76 |
| unambiguous interaction restraints | |
| UbcH8 | C85−SH |
| ubiquitin | C76−SH |

[a]Active residues represent those residues defined experimentally as being involved in the interaction from chemical shift perturbation (Figure 3C) or cross-saturation experiments (Figure 5C) and displayed more than 50% surface accessibility. [b]Passive residues are all neighboring residues of active residues that also show more than 50% surface accessibility. [c]The flexible segment is the known flexible region surrounding the active and passive residues on ubiquitin.

Table 2: Structural Statistics for the 16 Best UbcH8−Ubiquitin Model Structures

| | ensemble | representative structure |
|---|---|---|
| backbone rmsd (Å) with respect to mean secondary structure | 0.83 ± 0.26 | 0.58 |
| docking statistics | | |
| $E_{vdw}$ (kcal mol$^{-1}$) | −15 ± 3 | −16 |
| $E_{elec}$ (kcal mol$^{-1}$) | −127 ± 41 | −109 |
| $E_{avg}$ (kcal mol$^{-1}$) | −140 ± 30 | −125 |
| cluster population | 112 | − |
| AIR energy (kcal mol$^{-1}$) | 1.2 ± 0.3 | 1.2 |
| no. of AIR violations of >0.5 Å | 1.5 ± 0.2 | 1 |
| structural statistics | | |
| buried surface area (Å$^2$) | 815 ± 42 | 780 |
| rmsd from idealized covalent geometry | | |
| bonds (Å) | 0.004 ± 0.000 | 0.004 |
| angles (deg) | 0.654 ± 0.010 | 0.642 |
| impropers (deg) | 0.419 ± 0.010 | 0.415 |
| Ramachandran analysis | | |
| residues in the favored region (%) | 89.0 | 90.8 |
| residues in additional allowed regions (%) | 11.0 | 9.2 |

main ubiquitin binding site. Specifically, these interactions are found between I89, S90, and E92 on UbcH8, near the region where saturation transfer intensity decreases were noted (Figure 5), and R74, G75, and C76 on Ub.

## DISCUSSION

The E2−Ub thiolester intermediate is a central component of the ubiquitination pathway, yet there is limited structural information about the interactions within this complex or with an E3 ligase. The majority of the structural information comes from two E2−Ub complexes: Ubc1−Ub (*11*) and Ubc13−Ub (*37*). In the Ubc1−Ub complex, the thiolester formed directly in the NMR tube had limited stability ($T_{1/2} \sim 1$ h) and could not be purified from other reaction components (Ub, E1, ATP, and MgCl). This precluded assignment of resonances in the complex state and limited the thiolester analysis to broadening of the Ubc1 and Ub resonances in $^1$H−$^{15}$N HSQC spectra as a measure of mapping the interface (*11*). In the Ubc13−Ub complex, the active-site cysteine in Ubc13 was modified to a serine, allowing a more stable ester linkage to be formed between the two proteins, facilitating the determination of its structure by X-ray crystallography (*37*).

In this work, the E2−Ub complex was assembled using a disulfide to link the catalytic cysteine (C85) in UbcH8 to the C-terminus of Ub where a cysteine residue replaced the native glycine. The advantage of the disulfide linkage, like the ester linkage in the Ubc13−Ub complex (*37*), is that the UbcH8−Ub$^{Cys}$ complex can be purified from other components in a reaction mixture and is stable in solution for months. Previous work by our group has shown the disulfide linkage can be formed between Ub$^{Cys}$ and different E2 enzymes, including Ubc1, UbcH7 (UBE2L3), and Ubc13 (UBE2N) (*14*). In the case of Ubc1, it was shown that changes in the $^1$H−$^{15}$N HSQC spectra upon formation of the Ubc1−Ub$^{Cys}$ complex were nearly identical to those for the Ubc1−Ub thiolester, indicating that the disulfide is an appropriate structural mimic for the thiolester. The complete assignment of resonances in the UbcH8−Ub$^{Cys}$ complex and secondary structure analysis showed the formation of the complex does not result in major structural changes in either protein, a result similar to that observed for the Ubc13−Ub complex (*37*). This approach allowed chemical shift perturbation and saturation transfer experiments, in conjunction with the docking program HADDOCK, to be used to generate a family of structures for the UbcH8−Ub$^{Cys}$ complex.

*A Unique UbcH8−Ub Interface Is Formed.* The structure of the UbcH8−Ub$^{Cys}$ intermediate positions Ub$^{Cys}$ on the α3 helix and linker region preceding α5 (Figure 6), near the active-site cysteine (C85). In this orientation, contacts are made between C85−E92, I116−L120, and M122 of UbcH8 and T7−K14, Q31, D32, E34, Q41, and R72−C76 of Ub. The UbcH8−Ub$^{Cys}$ structure had a total combined buried surface area at the interface of 815 Å$^2$. It is apparent that Ub$^{Cys}$ occupies a different position in the UbcH8−Ub$^{Cys}$ structure compared to those in the Ubc13−Ub and Ubc1−Ub structures. In the Ubc1−Ub model, Ub is positioned on α2 and the preceding linker containing the catalytic cysteine (C88) in E2 (*11*). The α2 region in Ubc1 corresponds to an area on UbcH8 (α4, V103−R113) in which some of the smallest chemical shift and cross-saturation transfer changes occurred, indicating Ub does not occupy this site. Further, the buried surface area calculated from our UbcH8−Ub$^{Cys}$ structure is less than half the 1823 Å$^2$ surface area observed in the Ubc1−Ub model (*11*), indicating a looser arrangement likely exists between UbcH8 and Ub$^{Cys}$ in the complex. The Ubc13−Ub crystal structure orients Ub in the L4 linker and preceding loop−α3 region on the N-terminal side of the catalytic cysteine (*37*). The 647 Å$^2$ buried interface surface area obtained from the Ubc13−Ub structure (*37*) is much more comparable to that obtained from the UbcH8−Ub$^{Cys}$ structure. The differential

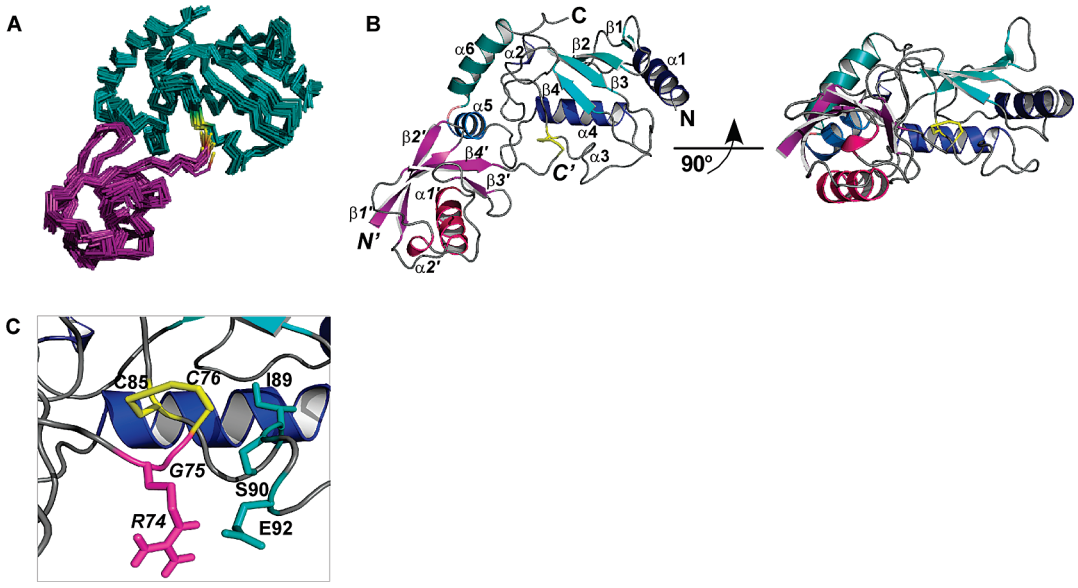


FIGURE 6: Model of the UbcH8−Ub$^{Cys}$ complex. (A) Superposition of the ensemble of the 16 lowest-energy structures in the most populated cluster as calculated from HADDOCK docking. (B) Ribbon drawing of the representative structure of the complex closest to the mean structure. The secondary structures in UbcH8 (turquoise) and Ub (magenta) are labeled and numbered with respect to the original PDB X-ray structures. (C) Detailed view of the UbcH8−Ub$^{Cys}$ binding interface showing side chain interactions between R74 (Ub) and E92 (UbcH8). The disulfide linkage between UbcH8 (C85) and Ub$^{Cys}$ (C76) is depicted as a yellow stick representation.

positioning of Ub on Ubc13 as compared to the UbcH8−Ub$^{Cys}$ structure may be due to the influence of the extensive interactions between Ub and the bound Mms2 conjugating enzyme variant in the Ubc13/Mms2 heterodimer. In this instance, the observed variations in the regions occupied by Ub on Ubc13 and UbcH8 might be expected. The surface on Ub that is occupied by each of these E2s is also interesting to note. Both UbcH8 and Ubc13 bind a similar region on Ub encompassing the loop following α1, the $\beta$1 strand, and the C-terminal tail (Figure S1 of the Supporting Information). Ubc1 appears to interact with a different region on Ub (R42, L43, and R48) that did not show chemical shift or saturation transfer sensitivity for the UbcH8−Ub$^{Cys}$ complex.

The unique positioning of Ub$^{Cys}$ on UbcH8 in our calculated structure is further supported by analyses of the electrostatic contributions and structural features of E2 catalytic domains. UbcH8 has a notably distinct electrostatic surface potential when compared to other E2 family members (*10*), including Ubc1 and Ubc13. In UbcH8, a distinct negative potential region exists on UbcH8 that includes the linker between $\beta$4 and α3, the linker preceding α4, and the linker preceding α5 (*10*). This region agrees well with the location of Ub$^{Cys}$ on UbcH8 in our structure. Moreover, the electrostatic surface potentials of Ubc1 and Ubc13, although different from those of UbcH8, are negative in regions where Ub has been shown to bind to each respective E2 (*10*). The difference on UbcH8 may also provide some insight into the dual role of UbcH8 in coordinating not only Ub but also the Ub-like protein ISG15 in their respective pathways (*38*).

The results from our work and previous studies provide evidence for the positioning of Ub in a specific location on each of the E2s. Previous studies show the E1 binding site on the E2 Ubc12 encompasses the N-terminal helix (α1) and the loop between strands $\beta$1 and $\beta$2 (*39*) (Figure 7). A similar location for E1 binding is expected for UbcH8, UbcH5c, and other E2 enzymes based on sequence similarity (*39*). The UbcH8−Ub$^{Cys}$ structure presented here positions the Ub away from the E1 binding site, leaving access to the UbcH8−Ub linkage for subsequent transfer to another E3 enzyme or substrate. Further,

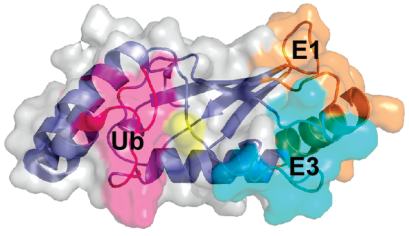


FIGURE 7: Surface map of E1, E3, and Ub binding surfaces on UbcH8 during ubiquitination. The UbcH8 structure is depicted as both a ribbon and transparent surface representation colored gray. The surface shows the Ub binding surface based on this work (magenta), the E1 binding surface based on the Ubc12−Uba1 structure (orange), and the E3 binding surface based on the UbcH7−c-Cbl structure (cyan).

an alternate location for the Ub closer to the α4 linker and $\beta$4 region on UbcH8, as seen in an alternate HADDOCK cluster (although the S−S distance between C85 in UbcH8 and C76 in Ub is violated), would likely interfere with the observed E1 binding site. Recently, it was shown that recruitment of E2 to the ubiquitin fold domain (UFD) on the Ub (or Ub-like protein)-charged E1, Uba1, promotes a conformational rotation of the UFD allowing the catalytic cysteines on both E1 and E2 to move closer to each other (from ~38 to ~8 Å) and facilitate transfer of Ub to the E2 (*39*, *40*). On the basis of our structure, the calculated position of Ub on UbcH8 would allow for the E1 to associate with the E2 and pass Ub to the active-site C85 on UbcH8 during ubiquitination.

Figure 7 also shows that the Ub binding site on UbcH8 does not interfere with the E2−E3 association as observed in X-ray and NMR studies. The RING-E3 c-Cbl in complex with the E2 UbcH7 shows the E3 contacting the L1−L2 loops (F63, K96, P97, and A98) and α1 (R6 and K9) on the E2 (*41*, *42*). The high degree of sequence similarity (72%) between UbcH7 (UBE2L3) and UbcH8 (UBE2L6) suggests similar residues in UbcH8 facilitate the E3 interaction surface. As with the E1 binding site, this location on UbcH8 is on the opposite side of the catalytic

cysteine away from the Ub binding site (Figure 7). This orientation on UbcH8 would allow binding of a thiolester-loaded UbcH8 with an E3 during progression of the ubiquitination pathway. Our results indicate that Ub is uniquely positioned on UbcH8 compared to other Ub−E2 intermediate complexes. This may indicate that differential positioning of Ub aids in the assembly with an E3 enzyme or substrate protein. Further, E2−Ub structures combined with biological experiments should help define how these complexes may provide an additional level of specificity in the ubiquitination pathway.

## ACKNOWLEDGMENT

We are grateful to Drs. P. Robinson and H. Ardley (University of Leeds, Leeds, U.K.) for the pGET-3a vector used in UbcH8 expression, Kathryn Barber for her excellent technical assistance, and Qin Liu for maintenance of the NMR spectrometers. We thank the Canadian National High Field NMR Centre (NANUC) for their assistance and use of the facilities. Operation of NANUC is funded by the Canadian Institutes of Health Research, the Natural Science and Engineering Research Council of Canada, and the University of Alberta.

## SUPPORTING INFORMATION AVAILABLE

Cross-saturation spectra of Ub in the UbcH8−$Ub^{Cys}$ disulfide with affected residues mapped onto the surface structure. This material is available free of charge via the Internet at http://pubs.acs.org.

## REFERENCES

1. Hershko, A., and Ciechanover, A. (1998) The ubiquitin system. *Annu. Rev. Biochem. 67*, 425–479.
2. Ciechanover, A., Orian, A., and Schwartz, A. L. (2000) Ubiquitin-mediated proteolysis: Biological regulation via destruction. *BioEssays 22*, 442–451.
3. Ciechanover, A., and Brundin, P. (2003) The ubiquitin proteasome system in neurodegenerative diseases: Sometimes the chicken, sometimes the egg. *Neuron 40*, 427–446.
4. Nalepa, G., Rolfe, M., and Harper, J. W. (2006) Drug discovery in the ubiquitin-proteasome system. *Nat. Rev. Drug Discovery 5*, 596–613.
5. Zhang, Y., Gao, J., Chung, K. K., Huang, H., Dawson, V. L., and Dawson, T. M. (2000) Parkin functions as an E2-dependent ubiquitin-protein ligase and promotes the degradation of the synaptic vesicle-associated protein, CDCrel-1. *Proc. Natl. Acad. Sci. U.S.A. 97*, 13354–13359.
6. Brzovic, P. S., Keeffe, J. R., Nishikawa, H., Miyamoto, K., Fox, D., III, Fukuda, M., Ohta, T., and Klevit, R. (2003) Binding and recognition in the assembly of an active BRCA1/BARD1 ubiquitin-ligase complex. *Proc. Natl. Acad. Sci. U.S.A. 100*, 5646–5651.
7. Kumar, S., Kao, W. H., and Howley, P. M. (1997) Physical interaction between specific E2 and Hect E3 enzymes determines functional cooperativity. *J. Biol. Chem. 272*, 13548–13554.
8. Burroughs, A. M., Jaffee, M., Iyer, L. M., and Aravind, L. (2008) Anatomy of the E2 ligase fold: Implications for enzymology and evolution of ubiquitin/Ub-like protein conjugation. *J. Struct. Biol. 162*, 205–218.
9. Winn, P. J., Religa, T. L., Battey, J. N., Banerjee, A., and Wade, R. C. (2004) Determinants of functionality in the ubiquitin conjugating enzyme family. *Structure* (*Cambridge, MA, U.S.*) *12*, 1563–1574.
10. Winn, P. J., Zahran, M., Battey, J. N., Zhou, Y., Wade, R. C., and Banerjee, A. (2007) Structural and electrostatic properties of ubiquitination and related pathways. *Front. Biosci. 12*, 3419–3430.
11. Hamilton, K. S., Ellison, M. J., Barber, K. R., Williams, R. S., Huzil, J. T., McKenna, S., Ptak, C., Glover, M., and Shaw, G. S. (2001) Structure of a conjugating enzyme-ubiquitin thiolester intermediate reveals a novel role for the ubiquitin tail. *Structure 9*, 897–904.
12. Dev, K. K., van der Putten, H., Sommer, B., and Rovelli, G. (2003) Part I: Parkin-associated proteins and Parkinson's disease. *Neuropharmacology 45*, 1–13.
13. Kitada, T., Asakawa, S., Hattori, N., Matsumine, H., Yamamura, Y., Minoshima, S., Yokochi, M., Mizuno, Y., and Shimizu, N. (1998) Mutations in the *parkin* gene cause autosomal recessive juvenile parkinsonism. *Nature 392*, 605–608.
14. Merkley, N., Barber, K. R., and Shaw, G. S. (2005) Ubiquitin manipulation by an E2 conjugating enzyme using a novel covalent intermediate. *J. Biol. Chem. 280*, 31732–31738.
15. Gardner, K. H., and Kay, L. E. (1998) The use of $^{2}H$, $^{13}C$, $^{15}N$ multidimensional NMR to study the structure and dynamics of proteins. *Annu. Rev. Biophys. Biomol. Struct. 27*, 357–406.
16. Golovanov, A. P., Hautbergue, G. M., Wilson, S. A., and Lian, L. Y. (2004) A simple method for improving protein solubility and long-term stability. *J. Am. Chem. Soc. 126*, 8933–8939.
17. Kay, L. E., Keifer, P., and Saarinen, T. (1992) Pure absorption gradient enhanced heteronuclear single quantum correlation spectroscopy with improved sensitivity. *J. Am. Chem. Soc. 114*, 10663–10665.
18. Grzesiek, S., and Bax, A. (1992) Correlating backbone amide and side chain resonances in larger proteins by multiple relayed triple resonance NMR. *J. Am. Chem. Soc. 114*, 6291–6293.
19. Wittekind, M., and Mueller, L. (1993) HNCACB, a high sensitivity 3D NMR experiment to correlate amide proton and nitrogen resonances with the α-carbon and β-carbon resonances in proteins. *J. Magn. Reson., Ser. B 101*, 171–180.
20. Grzesiek, S., Anglister, J., and Bax, A. (1993) Correlation of backbone amide and aliphatic side-chain resonances in $^{13}C/^{15}N$-enriched proteins by isotropic mixing of $^{13}C$ magnetization. *J. Magn. Reson., Ser. B 101*, 114–119.
21. Delaglio, F., Grzesiek, S., Vuister, G. W., Zhu, G., Pfeifer, J., and Bax, A. (1995) NMRPipe: A multidimensional spectral processing system based on UNIX pipes. *J. Biomol. NMR 6*, 277–293.
22. Johnson, B. A., and Belvins, R. A. (1994) NMRView: A computer program for the visualization and analysis of NMR data. *J. Biomol. NMR 4*, 603–614.
23. Shuker, S. B., Hajduk, P. J., Meadows, R. P., and Fesik, S. W. (1996) Discovering high-affinity ligands for proteins: SAR by NMR. *Science 274*, 1531–1534.
24. Kupce, E., and Wagner, G. (1995) Wideband homonuclear decoupling in protein spectra. *J. Magn. Reson. 109*, 329–333.
25. Vijay-Kumar, S., Bugg, C. E., and Cook, W. J. (1987) Structure of ubiquitin refined at 1.8 Å resolution. *J. Mol. Biol. 194*, 531–544.
26. Hubbard, S. J., and Thornton, J. M. (1993) NACCESS , University College London, London.
27. Vriend, G. (1990) WHAT IF: A molecular modeling and drug design program. *J. Mol. Graphics 8*, 52–56.
28. Krissinel, E., and Henrick, K. (2007) Inference of macromolecular assemblies from crystalline state. *J. Mol. Biol. 372*, 774–797.
29. Koradi, R., Billeter, M., and Wuthrich, K. (1996) MOLMOL: A program for display and analysis of macromolecular structures. *J. Mol. Graphics 14*, 51–55.
30. DeLano, W. L. (2002) Unraveling hot spots in binding interfaces: Progress and challenges. *Curr. Opin. Struct. Biol. 12*, 14–20.
31. Brzovic, P. S., Lissounov, A., Christensen, D. E., Hoyt, D. W., and Klevit, R. E. (2006) A UbcH5/ubiquitin noncovalent complex is required for processive BRCA1-directed ubiquitination. *Mol. Cell 21*, 873–880.
32. Miura, T., Klaus, W., Gsell, B., Miyamoto, C., and Senn, H. (1999) Characterization of the binding interface between ubiquitin and class I human ubiquitin-conjugating enzyme 2b by multidimensional heteronuclear NMR spectroscopy in solution. *J. Mol. Biol. 290*, 213–228.
33. Takahashi, H., Nakanishi, T., Kami, K., Arata, Y., and Shimada, I. (2000) A novel NMR method for determining the interfaces of large protein-protein complexes. *Nat. Struct. Biol. 7*, 220–223.
34. Dominguez, C., Boelens, R., and Bonvin, A. M. (2003) HADDOCK: A protein-protein docking approach based on biochemical or biophysical information. *J. Am. Chem. Soc. 125*, 1731–1737.
35. Quadt-Akabayov, S. R., Chill, J. H., Levy, R., Kessler, N., and Anglister, J. (2006) Determination of the human type I interferon receptor binding site on human interferon-α2 by cross saturation and an NMR-based model of the complex. *Protein Sci. 15*, 2656–2668.
36. Dominguez, C., Bonvin, A. M., Winkler, G. S., van Schaik, F. M., Timmers, H. T., and Boelens, R. (2004) Structural model of the UbcH5B/CNOT4 complex revealed by combining NMR, mutagenesis, and docking approaches. *Structure* (*Cambridge, MA, U.S.*) *12*, 633–644.
37. Eddins, M. J., Carlile, C. M., Gomez, K. M., Pickart, C. M., and Wolberger, C. (2006) Mms2-Ubc13 covalently bound to ubiquitin reveals the structural basis of linkage-specific polyubiquitin chain formation. *Nat. Struct. Mol. Biol. 13*, 915–920.
38. Zhao, C., Beaudenon, S. L., Kelley, M. L., Waddell, M. B., Yuan, W., Schulman, B. A., Huibregtse, J. M., and Krug, R. M. (2004) The

UbcH8 ubiquitin E2 enzyme is also the E2 enzyme for ISG15, an IFN-α/β-induced ubiquitin-like protein. *Proc. Natl. Acad. Sci. U.S.A. 101*, 7578–7582.
39. Lee, I., and Schindelin, H. (2008) Structural insights into E1-catalyzed ubiquitin activation and transfer to conjugating enzymes. *Cell 134*, 268–278.
40. Huang, D. T., Hunt, H. W., Zhuang, M., Ohi, M. D., Holton, J. M., and Schulman, B. A. (2007) Basis for a ubiquitin-like protein thioester switch toggling E1-E2 affinity. *Nature 445*, 394–398.
41. Zheng, N., Wang, P., Jeffrey, P. D., and Pavletich, N. P. (2000) Structure of a c-Cbl-UbcH7 complex: RING domain function in ubiquitin-protein ligases. *Cell 102*, 533–539.
42. Huang, A., de Jong, R. N., Wienk, H., Winkler, G. S., Timmers, H. T., and Boelens, R. (2009) E2-c-Cbl recognition is necessary but not sufficient for ubiquitination activity. *J. Mol. Biol. 385*, 507–519.
43. Wishart, D. S., and Sykes, B. D. (1994) The $^{13}C$ chemical-shift index: A simple method for the identification of protein secondary structure using $^{13}C$ chemical-shift data. *J. Biomol. NMR 4*, 171–180.